Superconductivity 11 (2024) 100114

Contents lists available at ScienceDirect

Superconductivity

journal homepage: www.elsevier.com/locate/supcon

Review Article

Advancements in dynamic characteristics analysis of superconducting electrodynamic suspension systems: Modeling, experiment, and optimization

Huan Huang [a,b], Haitao Li [c,*], Tim Coombs [d], Hanlin Zhu [e], Yougang Sun [a,b], Guobin Lin [a,b], Junqi Xu [a,b], Jun Zheng [c]

[a] Key Laboratory of Railway Industry of Maglev Technology, Tongji University, Shanghai 201804, China
[b] National Maglev Transportation Engineering R&D Center, Tongji University, Shanghai 201804, China
[c] State Key Laboratory of Rail Transit Vehicle System, Southwest Jiaotong University, Chengdu 610031, China
[d] Department of Electrical Engineering, University of Cambridge, Cambridge CB3 0FA, UK
[e] Department of Electrical & Electronic Engineering, University of Bristol, Bristol BS8 1UB, UK

ARTICLE INFO

Keywords:
Superconducting electrodynamic suspension
Electromechanical coupling dynamics
Equivalent experimental methods
Electromagnetic damping
Coil track irregularities

ABSTRACT

Superconducting electrodynamic suspension (EDS) presents numerous advantages, including large suspension gaps, high lift-to-drag ratios, and lower requirements for track irregularities. Recent advancements in superconducting materials have further enhanced the feasibility of this technology, and hence multiple research institutions are actively developing and improving this high-speed rail technology. Superconducting EDS achieves passive suspension and guidance by the interaction between ground null-flux coils and onboard superconducting magnets, forming an electromechanical coupled system. Thus, electromechanical coupling modeling and equivalent experimental methods are essential in evaluating and optimizing this system. This article reviews the research on dynamic characteristics analysis of superconducting EDS, focusing on modeling and experimental methods. Firstly, it revisits the development history of superconducting EDS and the new opportunities brought by advancements in superconducting materials. Secondly, it discusses various modeling approaches for the suspension system, emphasizing their benefits and limitations. Thirdly, it describes equivalent experimental methods and their respective application scenarios. Then, it reviews important conclusions and possible optimization methods related to dynamic performance and electromechanical coupling research. Additionally, the sliding window method is introduced to improve computational efficiency in vehicle dynamics modeling. This article provides insights into the current state and future directions of superconducting EDS research, serving as a valuable reference for researchers and engineers.

Contents

* Corresponding author.
E-mail address: lihaitao@swjtu.edu.cn (H. Li).

https://doi.org/10.1016/j.supcon.2024.100114
Received 7 July 2024; Revised 19 August 2024; Accepted 22 August 2024
Available online 25 August 2024

1. Introduction

Magnetic levitation (Maglev) trains use linear motors for propulsion and power supply and employ the electromagnetic forces between the vehicle-mounted magnets and the ground coils to counteract gravity. This technology allows for high speeds, strong climbing capability, and a small turning radius, that shows great potential for high-speed transportation. Electrodynamic Suspension (EDS) vehicles have the characteristics of large air gaps and self-stabilization, strong route adaptability, and low carbon emissions relative to aircraft [1], which was first proposed by Powell and Danby [2] of the Brookhaven National Laboratory in 1966. Japanese National Railways (JNR) started to develop superconducting EDS trains around 1970 [3]. Over 45 years, the first-generation vehicle series L0 set a world record speed of 603 km/h for manned rail transport in 2015, as depicted in Fig. 1(a). Series L0 improved version started running in 2020, as depicted in Fig. 1(b) and fully adopted the inductive power transmission method. Their efforts are directed towards developing a maglev system that speeds up to 500 km/h. This ambitious project is on track for completion, with plans to operate on the Tokyo-Nagoya route by 2034 [4].

1.1. EDS development with the promotion of superconducting materials

Superconducting magnets (SCMs) and their refrigeration systems are the core components of the EDS train. Therefore, the development of superconducting materials has a critical impact on the development of vehicle suspension structures.

In the series L0 vehicles, low-temperature superconducting (LTS) magnets are used. The LTS magnets, which predominantly utilize Nb-Ti wire, operate within the liquid helium temperature of 4.2 K, leading to high cooling costs and limiting wider research and development of EDS trains. Consequently, high-temperature superconducting (HTS) magnets, such as Bi2223 and RE123 tape, have emerged as a critical strategy in reducing cooling expenses and enhancing the commercial viability of EDS trains [5], as shown in Table 1. Using Bi2223 tape to replace Nb-Ti wire for onboard magnets increases the operational temperature from 4 K to 20 K. This transition allows for smaller, less powerful refrigeration units for conduction cooling, thus eliminating the need for a liquid helium compressor, and an additional electromagnetic radiation shielding device et al. An example of this advancement is seen in a full-size Bi-magnet system operating at 15 K, enabling the train to achieve a top speed of 553.9 km/h Yamanashi Maglev Test Line [6]. In 2015, Mizuno et al. [7] at the Railway Technical Research Institute (RTRI) successfully fabricated a full-scale pancake magnet with ReBCO tape. At cooling temperatures of 35 K and 32 K, the magnetomotive forces (MMFs) of the magnets reached 700 kA and 750 kA, respectively. The cooling power consumption is reduced by approximately 40 % compared to low-temperature Nb-Ti magnets.

In recent years, with the development of high-temperature SCMs, the requirements for refrigeration systems have gradually decreased, and the commercial application of EDS has been promoted. Research on EDS vehicles has also been gradually carried out in various countries. The Korea Railroad Research Institute (KRRI) started laying the groundwork for the subsonic tube train HyperTube in 2019 [10], and established a scaled test line for SCMs and propulsion motors [11,12], as shown in Fig. 2.

In January 2023, a superconducting navigation test was completed on a full-scale test line of the ultra-high-speed, low-vacuum tube maglev transportation system based on HTS tape by the 3rd research division of China Aerospace Science & Industry Corp. (CASIC), as illustrated in Fig. 3(a) [13]. In September 2023, a milestone was achieved with the completion of a commercial space electromagnetic launch featuring HTS EDS. This flight test, depicted in Fig. 3(b), reached a test speed of 234 km/h [14].

In December 2023, CRRC Changchun Railway Vehicles Co., Ltd. completed a comprehensive test system, successfully carrying out its initial operation, as illustrated in Fig. 4 [15]. It comprehensively encompassed HTS magnets, linear synchronous motors, inductive power supply, and single-stage low-temperature cooling. These achievements mark a critical advancement in high-speed rail transportation, showcasing the potential for more efficient and advanced rail systems.

1.2. Structure and operation principle of EDS train

Fig. 5 shows the structure of a superconducting EDS train. The side walls of the “U”-shaped track are continuously arranged with propulsion coils (PCs) and 8-shaped levitation and guidance coils

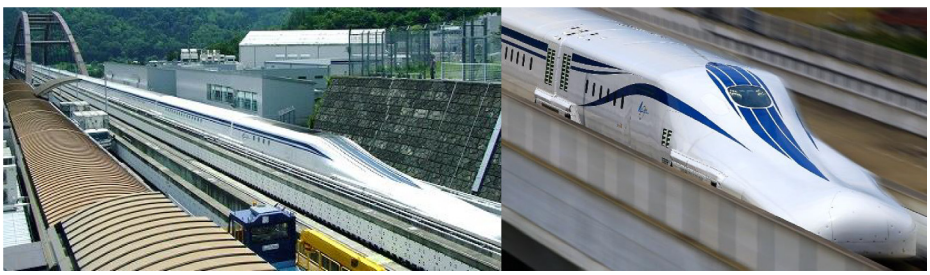

(a) Series L0 Version (b) Series L0 Improved Version

Fig. 1. Superconducting EDS Train on Yamanashi Test Line in Japan [4].

Table 1
LTS and HTS magnets for EDS train [5,8,9].

Description	LTS	HTS	
Superconducting Material	Nb-Ti wire	Bi2223 tape	ReBCO tape
Schematic Diagram		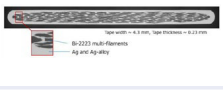	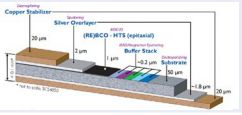
Onboard Magnets	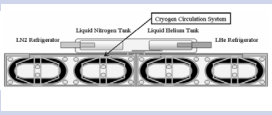	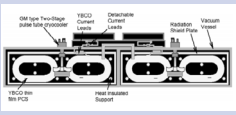	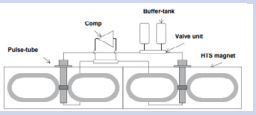
Operating Temperature	4.2 K	＜20 K	40 K~ 50 K
Cryogen and Cryocooler	Liquid N_2, Liquid He GM cryocooler GM/JT cryocooler	G-M type two-stage pulse tube cryocooler	Single-stage pulse tube cryocooler
Cooling Method	Pool Cooling	Conduction Cooling	Flow of gas He in cooling piping
Test Speed on Test Line	603 km/h	553.9 km/h	—

(a) Conceptual Diagram of HyperTube [10]

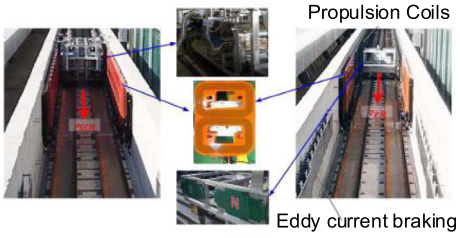

(b) Scaled Test Line and Propulsion Test [11]

Fig. 2. South Korea's EDS Layout and Scaled Test Line.

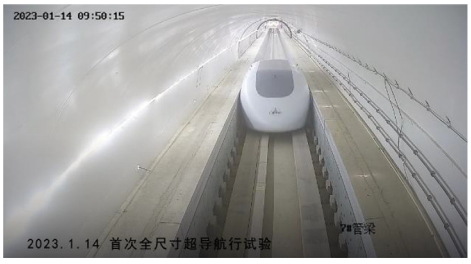

(a) Superconducting Navigation Test in January 2023 [13]

(b) Aerospace Electromagnetic Launch Flight Test in September 2023 [14]

Fig. 3. CASIC's High-Temperature Superconducting EDS Test.

(a) Test vehicle

(b) Test line

Fig. 4. CRRC Changchun's High-Temperature Superconducting EDS Test System [15].

(LGCs). The vehicle's suspension bogie carries SCMs and cryogenic containers (each suspension bogie has four SCMs on each side). The central maximum magnetic field of the onboard SCMs on the MLX01 series exceeds 5 T [16].

The electromagnetic coupling between the ground coils and the moving onboard SCMs produces electromagnetic forces, achieving the vehicle's levitation, guidance, and propulsion, as shown in Fig. 6. The onboard SCMs and the ground PCs form a long-stator linear synchronous motor, that propels the vehicle, as illustrated in Fig. 6 (a). By partition controlling the current in the ground coils, these windings sequentially become electromagnetic magnets with north and south poles. The levitation force of the superconducting EDS train comes from the onboard SCMs and the ground 8-shaped LGCs with their upper and lower loops connected in reverse, as shown in Fig. 6 (b). These coils, also called null-flux coils (NFCs), maintain zero magnetic flux when perfectly aligned with the SCMs. When the train operates at the take-off speed (usually 150 km/h), the suspension bogie sinks and the geometric center of the onboard SCMs deviates vertically from the center of the 8-shaped coils (typically by several centimeters). Guidance ensures the train remains centrally aligned without contacting the track. This is achieved by interconnecting the 8-shaped coils on two sides, which balance the electromagnetic forces to center the train, as shown in Fig. 6(c).

The electromagnetic forces with speed are shown in Fig. 7. As the speed increases, the levitation and guidance force first increases and then tends to saturation. However, the magnetic resistance is more prominent at low speeds and decreases significantly at high speeds.

1.3. Critical issues on dynamic characteristics of superconducting EDS train

Considering the integration of propulsion, suspension, and guidance systems, EDS exemplifies a typical electromechanical coupling system characterized by significantly nonlinearity with speed, position, and other operating parameters. The irregularity and the discrete arrangement of the coil-type track affect the stability of the train and the magneto-thermal stability of the SCMs, ultimately affecting operational safety and passenger comfort. It's crucial to couple the circuit and the dynamic equations to accurately analyse the dynamic characteristics, which significantly enlarges the computational matrix. The complexity of these systems necessitates innovative modeling approaches to manage the computational demands of high-speed operations.

Researchers have conducted extensive studies using various approaches considering the electromechanical coupling dynamic characteristics of superconducting EDS trains, each presenting unique benefits and limitations. On the other hand, electromechanical coupling calculations and operational tests are interdependent and progressive processes. A well-conceived computational model will guide the construction of the experimental platform, while experimental data will validate the theoretical model. However, achieving levitation in EDS trains necessitates specific speeds, and constructing experimental lines is costly and requires substantial space. Consequently, equivalent experimental methods and devices become crucial during the R&D stage. The following parts synthesize the research on dynamics analysis in superconducting EDS systems, evaluate different methodologies, and identify their strengths and weaknesses. It also proposes potential areas for optimization.

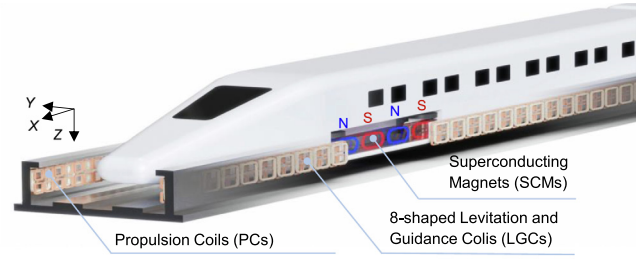

Fig. 5. Schematic Diagram of Superconducting EDS Track and Onboard Magnets.

2. Modeling method for electromagnetic characteristics of EDS train

The electromagnetic coupling mechanism between the ground 8-shaped LGCs and the onboard SCMs is crucial for establishing the dynamic magnetic-track relationship. Researchers like Murai et al. from RTRI [17] have published the test results of the time-domain electromagnetic forces in integrated Propulsion, Levitation, and Guidance (PLG) coils on the Miyazaki test line. Fujimoto et al. [18] have also reported the electromagnetic force test results from the Yamanashi Maglev test line. However, the data volume reported and the operational conditions covered by the experimental test are relatively small. Therefore, mathematical models of electromagnetic characteristics are required for structural design and optimization. There are two common methods for electromagnetic analysis: numerical calculation methods based on dynamic circuit theory [19–22] and finite element analysis [23–25], respectively. Each has its advantages and limitations.

2.1. Numerical calculation methods based on dynamic circuit theory

He et al. [21] in Argonne National Laboratory first applied the dynamic circuit theory to maglev systems. They established a dynamic circuit model to represent the system's energy, power, and electromagnetic forces through equivalent circuit parameters that vary over time. This model consists of a group of cross-connected 8-shaped LGCs and a pair of on-board SCMs. The numbering is shown in Fig. 8(a). The equivalent circuit illustrated in Fig. 8(b), includes four branches.

Based on the equivalent circuit diagram and Kirchhoff's voltage law, the circuit differential equations describing the dynamic characteristics can be written as follows:

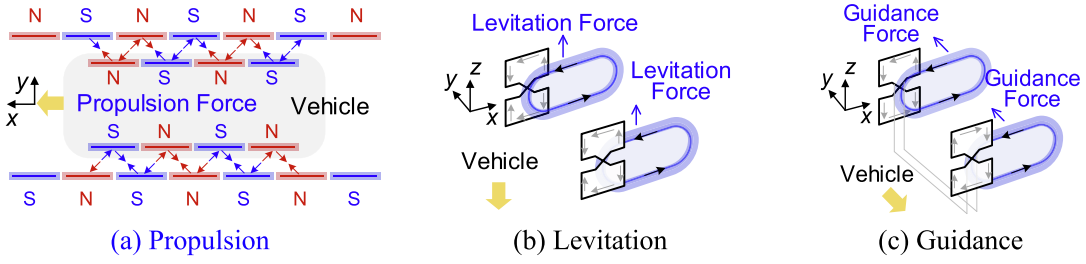

Fig. 6. Schematic diagram of the operation principle of superconducting EDS.

$$2Ri_1 + 2(L - M_{1,n+1})\frac{di_1}{dt} - Ri_{n+1} - (L - M_{1,n+1})\frac{di_{n+1}}{dt} = e_1 - e_{n+1} \quad (1)$$

$$-Ri_1 - (L - M_{1,n+1})\frac{di_1}{dt} + 2Ri_{n+1} + 2L\frac{di_{n+1}}{dt} - Ri_{2n+1} - (L - M_{2n+1,3n+1})\frac{di_{2n+1}}{dt} = e_{n+1} - e_{2n+1} \quad (2)$$

$$-Ri_{n+1} - (L - M_{1,n+1})\frac{di_{n+1}}{dt} + 2Ri_{2n+1} + 2(L - M_{2n+1,3n+1})\frac{di_{2n+1}}{dt} = e_{2n+1} - e_{3n+1} \quad (3)$$

where R and L are the resistance and inductance of each branch of 8-shaped LGCs. $M_{1,n+1,}$ and $M_{2n+1,3n+1}$ represent the mutual inductances between branches 1 and $n + 1$, $2n + 1$ and $3n + 1$, respectively. $M_{1,n+1} = M_{2n+1,3n+1} = M_{lg}$; i_1, i_{n+1}, i_{2n+1} are the currents in the three circuits loop in Fig. 8, respectively. e_j ($j = 1, n + 1, 2n + 1, 3n + 1$) is the induced electromotive force (EMF) in the j-th coil branch, calculated according to the following formula:

$$e_j = -I_s^1\left(v_x\frac{\partial M_{s,lg}^{(1,j)}}{\partial x} + v_y\frac{\partial M_{s,lg}^{(1,j)}}{\partial y} + v_z\frac{\partial M_{s,lg}^{(1,j)}}{\partial z}\right) \quad (4)$$

where I_s^1 represents the magnetomotive force of the 1st SCMs; $M_{s,lg}^{(1,j)}$ ($j = 1, n + 1, 2n + 1, 3n + 1$) represents the mutual inductances between the j-th branch of the LGCs and the SCMs on the same side.

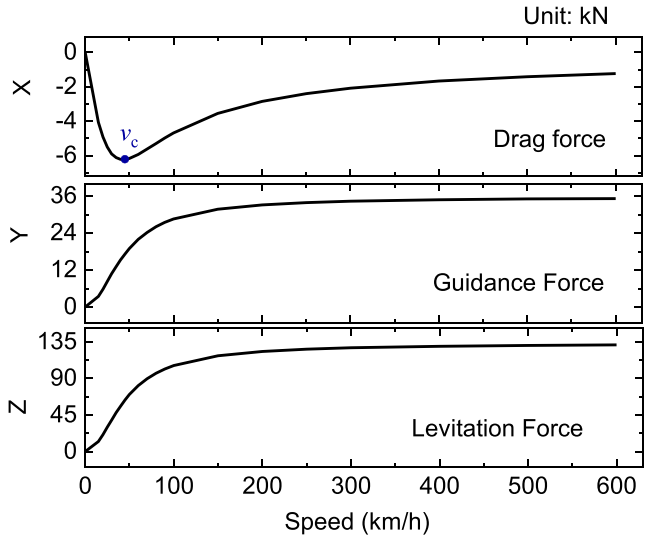

Fig. 7. The electromagnetic force of four onboard SCMs on one side of the suspension bogie as a function of vehicle speed.

Without considering lateral and vertical vibration, the velocities in the y and z directions can be disregarded. However, when considering lateral/vertical dynamics, it is necessary to account for the induced EMF generated by lateral/vertical vibration. After solving the above differential equation set for the circuit currents, the electromagnetic force $\boldsymbol{F}_{s,lg}^i$ and torque $\boldsymbol{T}_{s,lg}^i$ during the movement of the i-th SCM can be obtained based on the virtual displacement method as follows:

$$\boldsymbol{F}_{s,lg}^i = -I_s^1\sum_{j=1}^{3n+1} I_{lg}^j\frac{\partial \boldsymbol{M}_{s,lg}^{(1,j)}}{\partial \boldsymbol{X}} \quad (5)$$

$$\boldsymbol{T}_{s,lg}^i = -I_s^1\sum_{j=1}^{3n+1} I_{lg}^j\frac{\partial \boldsymbol{M}_{s,lg}^{(1,j)}}{\partial \boldsymbol{\alpha}} \quad (6)$$

where I_{lg}^j ($j = 1, n + 1, 2n + 1, 3n + 1$) is the induced current of the j-th branch of LGCs. $\boldsymbol{X} = [x \quad y \quad z]$, $\boldsymbol{\alpha} = [\theta \quad \phi \quad \psi]$.

Researchers have utilized dynamic circuit models to analyze multi-coil systems, which include LGC track with multiple onboard SCMs, cross-connected LGC track systems, and PLG track systems. Additional research efforts have further expanded and applied this model. Azukizawa [26] investigated the impact of harmonic components in LGCs on the SCMs' currents and the electromagnetic forces. In addition, by improving the model, the relationship between its dynamic electromagnetic characteristics [20,27–29] and parameters such as speed and lateral/vertical offsets is discussed in detail. The core focus of these dynamic circuit models is to solve the mutual inductance between the SCMs and the LGCs. The spatial Fourier method [30] and the Neumann formula [26] are two common methods.

(1) The spatial Fourier method

Nonaka et al. [31] applied the spatial Fourier method to analyze the spatial field distribution of onboard SCMs. The idea of this method is to periodically extend the SCM in space. Lv et al. [32,33] applied harmonic approximation to calculate the mutual inductance between the ground coils and SCMs, analyzing the averaged force and time-domain force characteristics of the EDS system under various vertical and lateral offsets. We improved and completed the spatial magnetic field distribution simulation of the racetrack SCMs [34] with the extension of the longitudinal x-axis and vertical z-axis, with periods of L_x and W_z, respectively, as shown in Fig. 9. To minimize the impact on the spatial magnetic field distribution of the SCMs, the vertical extension period W_z should be much larger than the magnet's width of $2b_0$. The spatial distribution of magnetic potential determines the boundary conditions of the Laplace equation for magnetic scalar potential or magnetic vector potential. By solving the Fourier expression of the magnetic potential distribution of the onboard SCMs, the magnetic flux density of the SCMs array after periodic extension can be obtained. By integrating the magnetic flux density in each 8-shaped LGC loop and dividing by the current I_s in the SCMs, the mutual inductance between the SCMs and various LGCs can be derived.

In practical applications, it's important to note that SCMs are generally composed of multiple layers of superconducting wire. Modeling

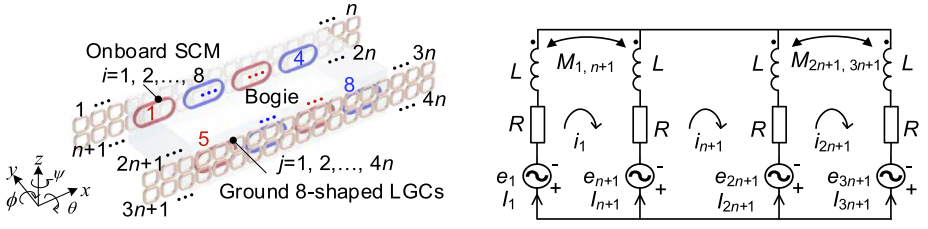

(a) Schematic diagram of suspension bogie (b) Equivalent circuit of one group of LGCs

Fig. 8. Schematic diagram of the equivalent circuit model.

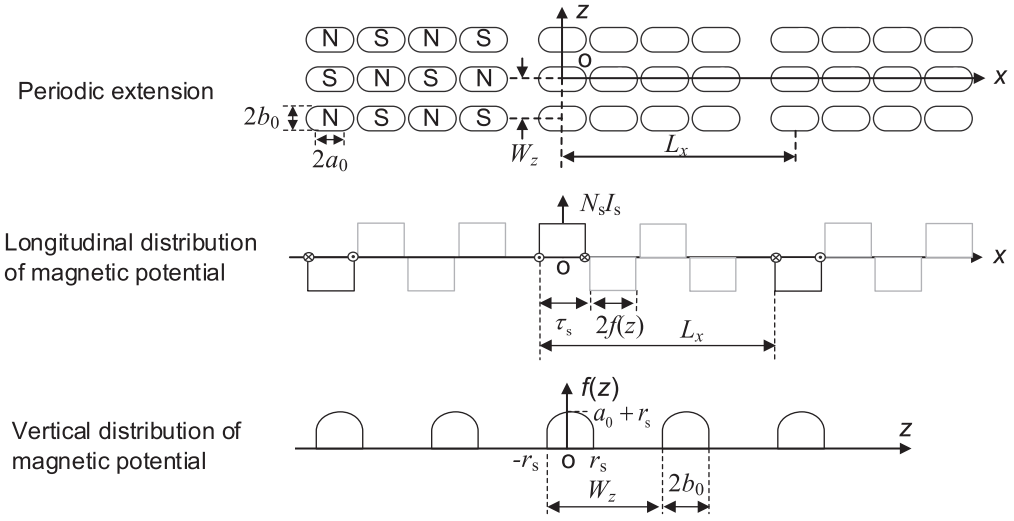

Fig. 9. Periodic Extension Model of SCMs based on spatial Fourier method.

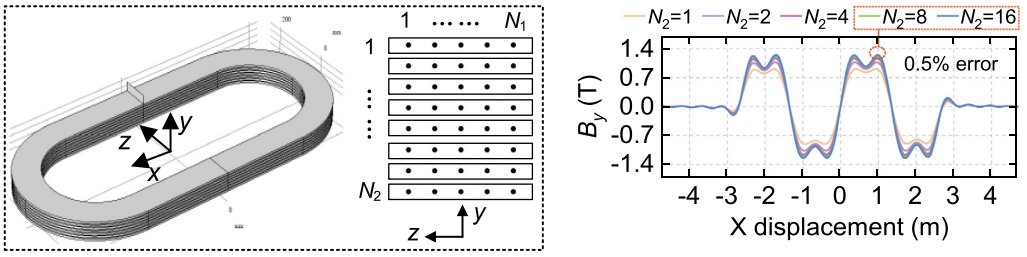

(a) Discretization of SCM cross-section (b) B_y with different N_2

Fig. 10. Schematic diagram of discretion of SCMs and calculation results of magnetic flux in *y*-direction.

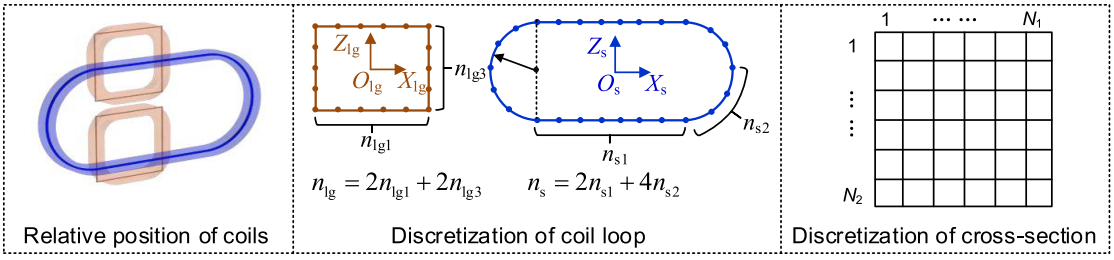

(a) Discretization of the coil loop and cross-section

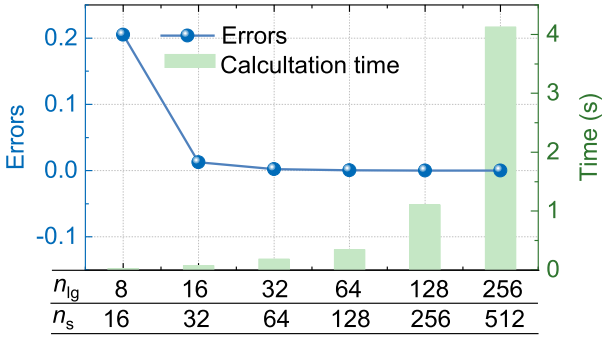

(b) Calculation time and errors with different discretization numbers

Fig. 11. Discretization of the coils and calculation time based on Neumann formula.

these coils as ideal (without any physical thickness) could significantly affect accuracy. Hence, the discretization of the coil's cross-section is necessary [30], as shown in Fig. 10. Upon analysis, SCMs divided into 8 and 16 layers showed only a 0.5 % difference in magnetic field. Consequently, opting to model SCMs with 8 layers is deemed appropriate, consistent with the typical configuration in HTS magnets with 8 pancakes [35], providing a reference for practical implementations.

The Fourier series method can be used to qualitatively understand electromagnetic characteristics, particularly the harmonic components of induced currents in LGCs. It serves well for harmonic analysis, power collecting coil, and damping coil design [36,37]. However, when addressing coupled nonlinear motions and large displacement motion equations, it's essential to consider the nonlinear relationships of the mutual inductance with the spatial position change of the bogie. Realistically representing spatial mutual inductance factoring into higher harmonics within feasible computation times becomes difficult. Hence, this approach has typically focused on average forces, which may not adequately capture the dynamic characteristics of the vehicles.

(2) Line Integration Based on Neumann's Formula

The Neumann formula, derived from the magnetic vector potential and Faraday's law of induction, provides an analytical solution of the mutual inductance as follows:

$$M = \frac{\mu_0}{4\pi} \oint_{L_2} \oint_{L_1} \frac{dl_1 \cdot dl_2}{R} \tag{7}$$

where $\boldsymbol{l}_1$ and $\boldsymbol{l}_2$ are the integral paths of two coils. However, due to its complexity, this formula is limited to analytically solving simple geometric configurations. In the electromechanical analysis of an EDS train with multiple bogies, the mutual inductance between two arbitrary-positioned and orientated polygonal coils should be estimated with reduced computational effort by solving the Neumann formula using numerical integration. To avoid the selection of integral path functions, Kim et al. [38] introduced a mesh matrix involving cross-section and elliptic integrals for the unit turn to calculate the mutual inductance for noncoaxial coupled coils. Following this methodology, Su et al. [39] discretized the cross-section and unit coordinate matrix for the coil loop central line, shown in Fig. 11(a). Subsequently, the mutual inductance between each discrete unit is calculated using Eq. (7) and then superimposed and coordinate-transformed to obtain the mutual inductance at any relative spatial position. The optimal number of discretization points $n_g = 32$, and $n_s = 64$ are determined considering both computational time and accuracy for effectively modeling the electromagnetic coupling between the 8-shaped LGCs and racetrack SCMs, as shown in Fig. 11(b). The advantage of this method is its high accuracy, making it suitable for calculating various irregular coils, leading to an efficient numerical solution for electromagnetic coupling of the EDS system.

2.2. Numerical simulation methods based on finite element analysis

Finite Element Method (FEM) is a modeling method suitable for accurately simulating complex structural systems. In EDS systems, challenges related to long tracks and simulating LGC configurations with cross-connected cables add complexity to FEM models. The distinct 8-shaped LGC structure makes it necessary to use a 3-D geometric model. Gong et al. [23] developed an advanced model of an EDS system with 8-shaped coils utilizing magnetic vector potential and equivalent circuit methods in COMSOL Multiphysics. This model avoids moving mesh for onboard SCMs thus achieving higher computational accuracy. However, using multiple LGCs in these models still leads to extended computation times, especially under high-speed operation conditions. The selection of dependent variables and boundary conditions can affect computational costs. The ***A*-*H*** hybrid formulation proposed by Brambilla et al. [40] and Santos et al. [41] has shown good stability in solving 2-D electromagnetic field problems of superconducting systems within COMSOL. For 3-D electromagnetic field problems involving linear motion, the magnetic scalar potential V within moving boundaries is suggested for precise and efficient calculations [42].

To address the long track and cross-connected 8-shaped LGC structure issues in 3-D models, we [25] employed vector-scalar magnetic potential, i.e. ***A*-*V*** hybrid formulation, and introduced field-circuit coupling methods and periodic conditions. The 3-D geometric model unit, as shown in Fig. 12, consists of two pairs of alternately polarized

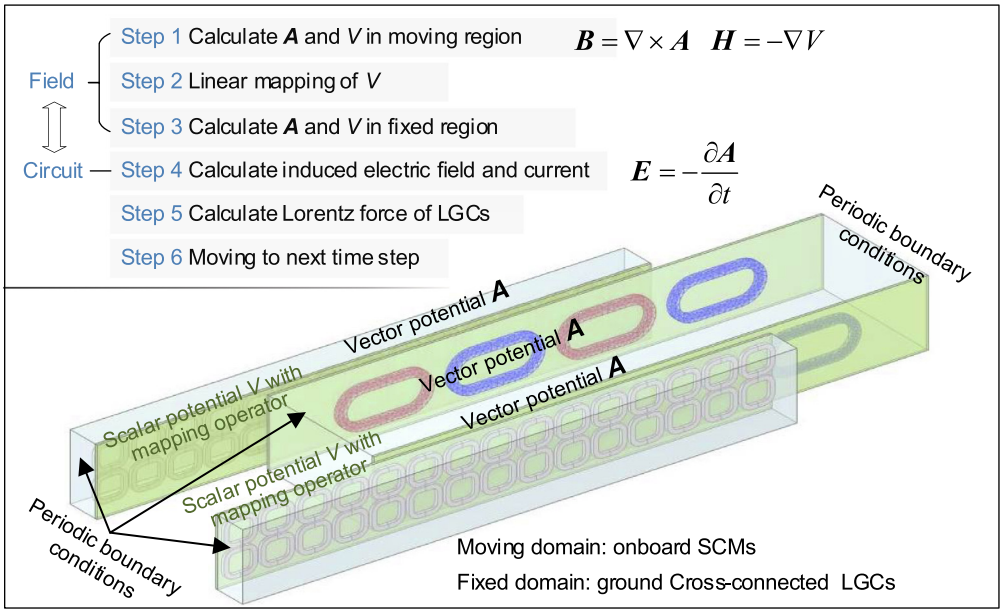

Fig. 12. The boundaries and calculation flow of FEM for EDS suspension bogie.

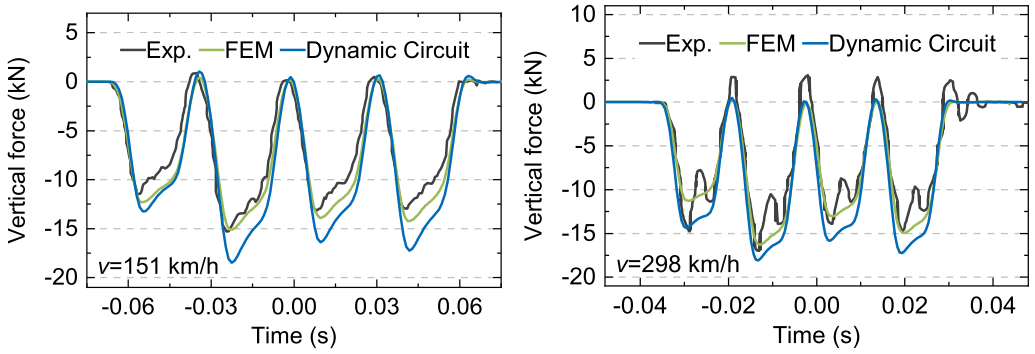

(a) v=151 km/h (b) v=298 km/h

Fig. 13. Time-domain vertical electromagnetic force on a single 8-shaped coil (The experimental data comes from the literature [18]).

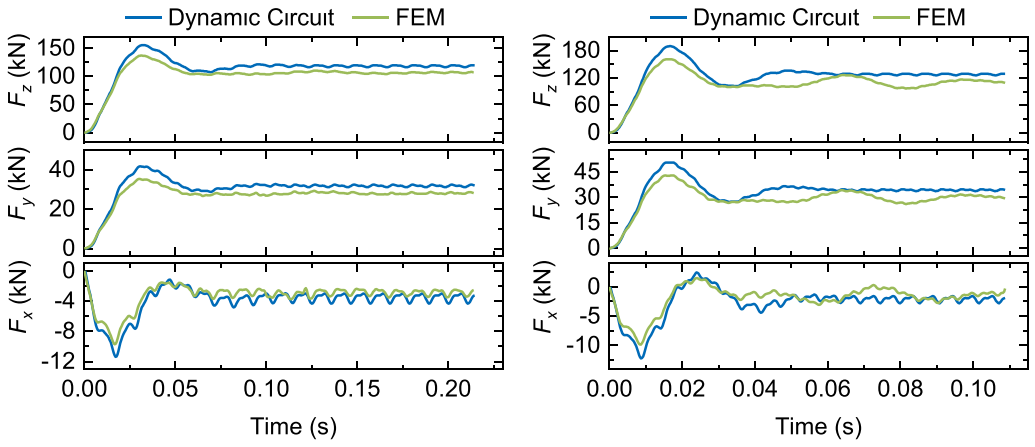

（a）v=151 km/h （b）v=298 km/h

Fig. 14. Time-domain electromagnetic force on one side of the suspension bogie.

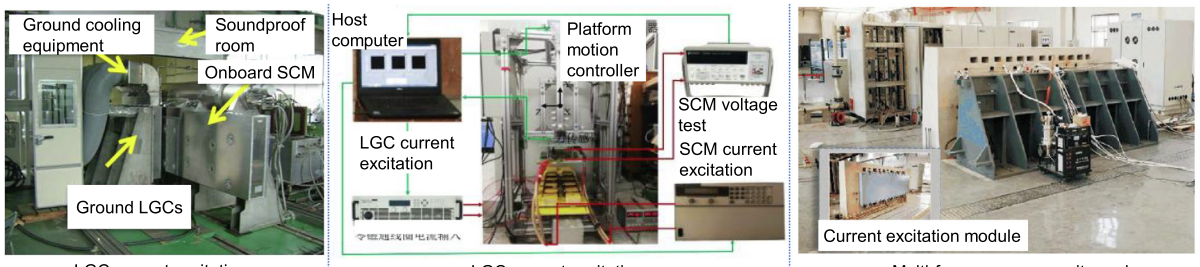

(a) RTRI, Japan (b) SWJTU, China (b) CASIC, China

Fig. 15. Static equivalence with the active current excitation test platform.

onboard SCMs in the moving domain, matched with twelve 8-shaped LGCs in the fixed domain. The moving and fixed domains form an assembly with contact boundaries to maintain continuity. A moving mesh is added to simulate the motion of SCMs.

2.3. Model comparison and evaluation

This section aims to compare and evaluate the electromagnetic forces generated by FEM simulations against those derived from the dynamic circuit model. Fig. 13 shows the vertical electromagnetic forces on a single 8-shaped LGC, comparing numerical simulations with experimental results. The operation conditions of simulations and experiments are the same: lateral and vertical displacements are 0 and −40 mm, and the operating speeds are 151 km/h and 298 km/h, respectively. The trends in both numerical models match the experimental results well. Notably, as each onboard SCM passes through the LGCs, the electromagnetic force curves are different, which is consistently reflected in the experimental and numerical data.

The electromagnetic force results from the two numerical models are slightly higher than the experimental results, and the error under high-speed conditions is smaller than that under low-speed conditions. Importantly, the difference noted in the FEM, which uses actual geometric structures is consistently lower than those in the dynamic circuit model across both speed conditions. This is because, in the solution of the dynamic circuit model, we did not consider the effects of cross-sectional size, thickness of coils, etc., and only considered the mutual inductance calculated as a single line loop.

Fig. 14 presents the time-domain electromagnetic forces of the four onboard SCMs on one side of the suspension bogie. The data indicate that the electromagnetic forces calculated via FEM are slightly smaller than those from the dynamic circuit model. The simulation results all reflect high-frequency vibration of electromagnetic force.

3. Equivalent experimental platform and experimental methods

Experiments are a vital method for investigating the electromechanical relationships between SCMs and LGCs and understanding how electromagnetic physical quantities impact these components. However, conducting full-scale experiments of superconducting EDS vehicles presents several significant challenges. Additionally, constructing a test vehicle and test line is costly, and currently, only Japan possesses the full-scale test vehicle and the Yamanashi test line, which limits the feasibility of conducting similar experiments in other locations. Model experiments often simplify complex operating conditions with a scale prototype. For instance, costly SCMs can be replaced with permanent magnets (PMs). Linear motion may be substituted with rotational motion and electromechanical coupling effects with electromagnetic interactions. Current EDS experimental platforms are categorized into three types: static equivalence with active current excitation, and dynamic simulation based on the Stewart platform, dynamic equivalence using rotational motion instead of linear motion.

3.1. Static equivalence of simulating passive current using active current excitation

Static equivalence experiments, where there is no relative motion between coils, achieve motion equivalence by converting it into AC excitation on LGCs. This method helps avoid mechanical oscillation errors caused by relative movement between SCMs and LGCs.

RTRI has developed an electromagnetic excitation vibration platform, shown in Fig. 15(a) [43]. Ground 8-shaped coils are installed opposite the excited SCMs. Utilizing a dedicated inverter power supply, where DC or AC across a range of frequencies and values can be applied, allowing for the simulation of electromagnetic vibrations. This experimental setup is primarily used for durability testing of LGCs [44] and electromagnetic-thermal stability testing of superconductors [45]. Unlike mechanical excitation, electromagnetic vibration can directly apply electromagnetic forces as distributed loads to conductors, enabling more precise and effective testing.

Ma et al. [46] from Southwest Jiaotong University (SWJTU), China, developed a similar system, depicted in Fig. 15(b), employing an analytical-experimental coupling approach to study the time-domain electromagnetic force at various speeds. Utilizing Neumann's formula-based model, they first calculate the induced currents in the LGCs. These calculated currents are then dynamically injected into the LGCs following the trajectory of the EDS train, with adjustments made to the relative positions of the superconducting magnets and LGCs.

Similarly, Hu et al. [47] from CASIC developed a double-layer excitation coil, as shown in Fig. 15(c). They use a multi-frequency composite current closed-loop control strategy to effectively simulate the spatial magnetic field distribution produced by the PCs and LGCs. The background spatial magnetic field, electromagnetic load, and vibration acceleration response of SCMs under both online operation and offline electromagnetic vibration simulations were simulated and compared.

3.2. Dynamic performance simulation based on the Stewart platform

RTRI and KRRI have employed six-degree-of-freedom Stewart motion platforms to simulate the dynamics of EDS vehicles composed of two-series suspension devices and vehicle bodies. Suzuki et al. [48] at RTRI constructed a 1/12 scale experimental device to investigate the coupled vibrations between the vehicle body and the bogies through active interaction forces. Experimental tests of control methods were conducted to suppress vibrations. Similarly, Lee et al. [49] at KRRI developed a 1/10 scaled Hyperloop vehicle model that includes a suspension bogie, secondary suspension devices, and a vehicle body, all operated by the Stewart platform.

Both of the aforementioned methods rely on numerical calculations to substitute the induced current/electromagnetic force generated by the relative movement of the onboard and ground coils. The accuracy of the experiments mainly depends on the accuracy of the numerical calculation methods, which is divorced from the essence of passive suspension.

3.3. Dynamic equivalence using rotational motion instead of linear motion

Using rotational motion to simulate linear motion can more accurately capture the dynamic electromagnetic forces without relying on simulation models. It is a crucial experimental approach for investigating dynamic electromagnetic characteristics and vibration behaviors.

Song et al. [50] at the National University of Defense Technology (NUDT) developed a single-sided EDS experimental device based on 8-shaped NFCs and PMs, as shown in Fig. 16. This system comprises a turntable motor, motor control system, and three-axis force sensors, operating within a speed range of 0–20 m/s. The electromagnetic forces with speed for different vertical offsets Δz and lateral air gaps δ are tested. Wang et al. [51] at SWJTU designed a prototype that

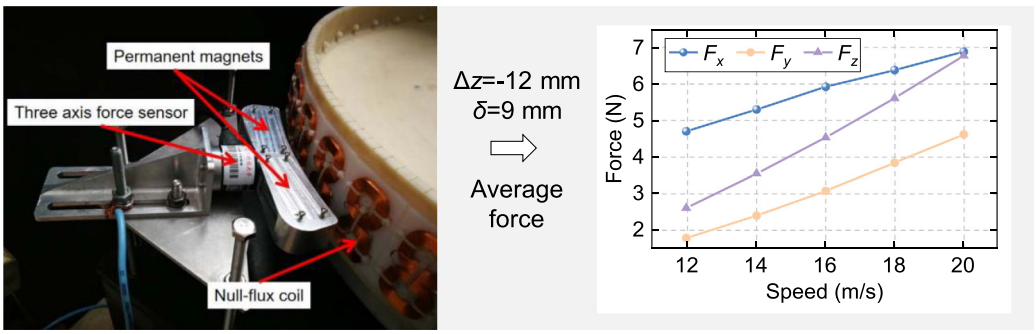

Fig. 16. One side PM-EDS platform and electromagnetic force test in NUDT, China [50].

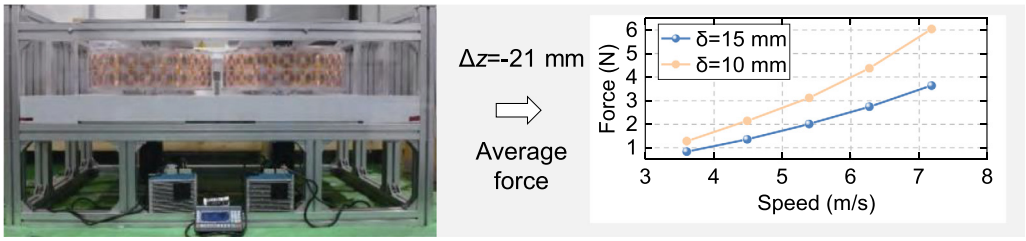

Fig. 17. Double-side PM-EDS test platform in SWJTU, China [51].

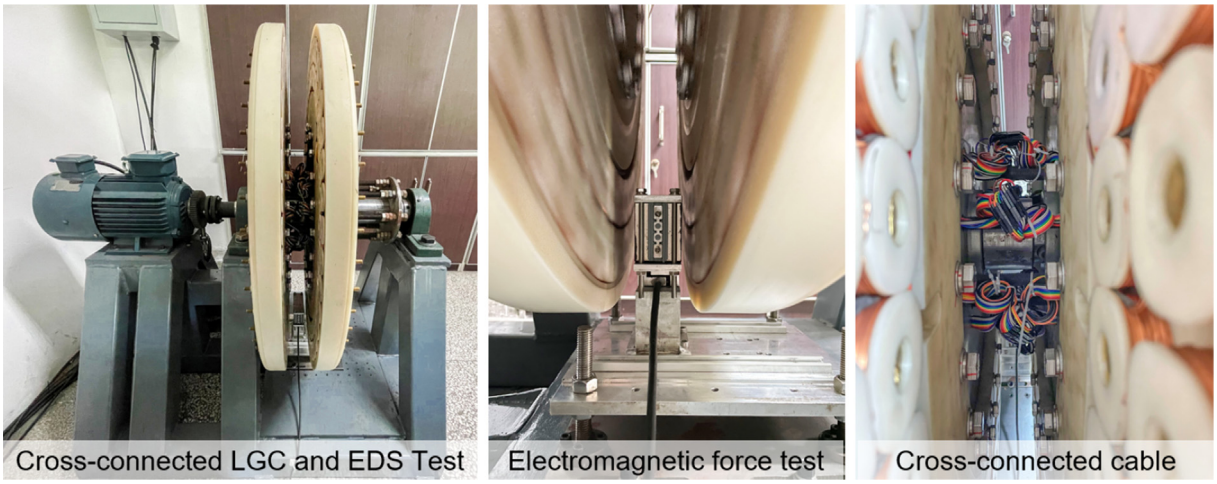

Fig. 18. Rotation EDS platform with cross-connected cable.

divides the NFCs into two groups and places them symmetrically on both sides of the PMs for bigger levitation force, as shown in Fig. 17. The NFCs on both sides are driven by stepper motors to rotate synchronously in opposite directions, simulating the two sides of NFCs.

The previously rotating test platforms can simulate the levitation force but do not account for the cross-connection of the system's two-side 8-shaped NFCs. To address this issue, our research group developed an equivalent cross-connected LGC EDS experimental platform, as shown in Fig. 18. Multiple coils are evenly distributed on the inner walls of the two turntable structures. Time-domain electromagnetic force and suspension vibration simulation at different speeds and lateral/vertical air gaps are under testing. This platform provided a new approach to the dynamic characteristics analysis of a cross-connected coil-type EDS system.

4. Dynamics and vibration control of superconducting EDS train

During operation, the EDS train faces disturbances from both external sources like track foundation settlement and LGC installation errors, and internal sources such as the discrete arrangement of ground LGCs and high-order harmonics of the PC's magnetic fields. Such disturbances can significantly impact the dynamic performance of the superconducting EDS train, affecting its stability and ride comfort. However, the damping coefficient of the coupling effect between the LGCs and the SCMs is negative [52–54], which makes it difficult to dissipate the vibration energy. Therefore, research on the vibration mechanism of superconducting EDS trains, and carrying out vibration suppress design and optimization are of great significance to ensuring the safe operation of EDS trains. Since the longitudinal operating speed is several orders of magnitude greater than the lateral and vertical vibration speed, this article does not analyze the coupling relationship between the propulsion system and dynamic performance. Instead, it focuses more on the aspects of lateral and vertical dynamics.

4.1. Stiffness and damping characteristics analysis

Yonezu et al. [55] explored how lateral/vertical offsets and MMF of SCMs affect the magnetic force stiffness, demonstrating a nonlinear relationship with stiffness properties, as shown in Fig. 19(a) and (b). For instance, at certain operation conditions, reduced gaps lead to increased equivalent lateral and rolling stiffnesses. Consequently, lateral deflection might induce lateral-rolling coupled vibrations. Simultaneously, Fig. 19 (c) demonstrates the negative damping characteristics of the suspension system. These findings highlight the importance of considering multi-degree of freedom coupling and the nonlinear interactions between electromagnetic forces and mechanical motions, especially on curved sections.

4.2. Dynamic magnetic-track relationships and dynamics of EDS train

The aforementioned models provide calculation methods for electromagnetic forces. Researchers use them to derive a constant stiffness by fitting the calculated electromagnetic forces, or store variable stiffness, electromagnetic forces, and mutual inductance values in a database for look-up.

Zhang et al. [29] established equivalent linear and nonlinear stiffness models and analyzed the influence of running speed and secondary suspension parameters on dynamic performance. Yonezu [55] applied a nonlinear stiffness model to research the impact of the lateral/vertical position and MMF on the dynamic characteristics. Yoon et al. [56] derived a nonlinear stiffness model with the running speed and lateral/vertical position and compared the vehicle dynamic behaviors of three types of LGC structures and the pole-pitch

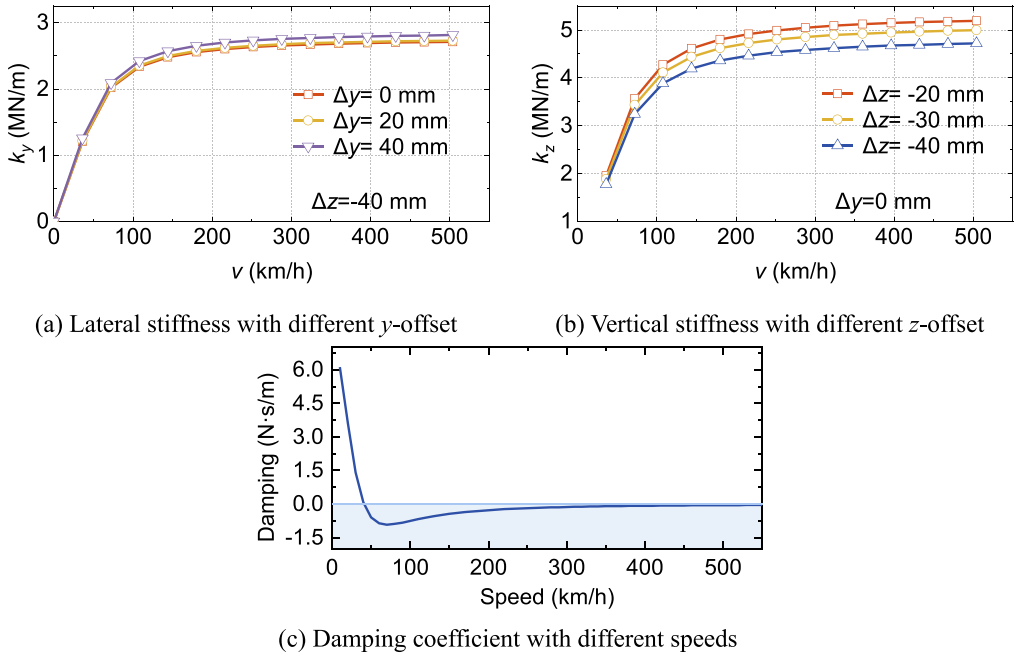

(a) Lateral stiffness with different *y*-offset

(b) Vertical stiffness with different *z*-offset

(c) Damping coefficient with different speeds

Fig. 19. Stiffness and Damping Characteristics with different speeds and positions.

configuration of the EDS train. Yu et al. [57] added harmonics to the electromagnetic force fitting curve to investigate high-frequency vibrations and analyze the vertical-pitching motion of EDS vehicles. The equivalent stiffness method uses linear or nonlinear curves, limited to dealing with multiple nonlinear factors. Alternatively, the look-up method creates a database of values like mutual inductance, stiffness, or electromagnetic force, sorted by speed and position. These values are then used in real-time to simulate dynamic behaviors during operation more accurately. Zhang et al. [58] and Ha et al. [59] established an electromagnetic force database related to speed and lateral/vertical position as the magnetic track relationship. Li et al. [60] established a database of mutual inductance at different lateral/vertical positions and discovered the nodding posture operation phenomenon caused by the uneven electromagnetic force of the onboard SCMs.

While the above methods enhance computational efficiency, but face challenges in the simulation of negative damping characteristics of the suspension bogie, high-frequency vibrations resulting from high harmonics of discrete LGCs and PCs, and uneven forces on SCMs due to current distribution differences. An electromagnetic-dynamic synchronous coupling solution method has been developed to address these issues. This method involves coupling the circuit equations with the dynamic equations to analyze the electromagnetic force and motion state in real time. Ohashi et al. [61] established an electromagnetic-dynamic coupling model of suspension bogie considering PCs, LGCs, and SCMs. Tan et al. [62] further explored this method by analyzing the dynamic performance of a Π-shaped track EDS system. Ma and Yan [63] confirmed that the coupling simulation method is less computationally efficient but provides more accurate dynamic performance. Su et al. [64] enhanced the variable stiffness model's efficiency by incorporating a neural network to predict the relationship between the onboard SCM's spatial attitude and its electromagnetic characteristics.

4.3. Primary vibration control strategies

The coil-type EDS train integrates an electromagnetic system featuring coiled components with a mechanical system governing vehicle motion. The electromechanical coupling characteristics are also the sources of vehicle vibrations. Consequently, integrating a vibration suppression system based on the electromechanical coupling effect is essential to enhance the vehicle's dynamic performance. There are two main categories of vibration suppression based on electromechanical coupling: one involves implementing active current control within the LGCs, and the other involves introducing onboard electromagnetic damping in the suspension system.

(1) Implementing Active Current Control within the Electromagnetic Coils

In EDS systems, various electromagnetic coils provide potential actuators for vibration control. Sakamoto and Nakayama [65] controlled the current in the LSM armature to provide auxiliary forces, improving levitation and guidance performances under crosswinds and low speeds. Boeij et al. [66] established a real-time control model for a 5-degree-of-freedom dynamics of the EDS sled equipped with NFCs. They successfully controlled the multi-degree-of-freedom vibration of the passive sled through active current modulation of the NFCs. Subsequently, Gutierrez and Luijten [67] adopted a sliding mode controller with a nonlinear input mapping from coil current to electromagnetic force, actively suppressing disturbances unrelated to the sled velocity. Li et al. [60] proposed a method that uses different magnetomotive forces in different SCMs to improve the pitch motion of the suspension bogie. While these approaches are theoretically feasible, most have been validated using scale models or simulations. They may not be practical or economical from an operational and cost-efficiency standpoint. Implementing active current control along the entire track would require numerous power sources and controllers and real-time monitoring of vehicle dynamics with feedback to the track, demanding high immediacy in communications.

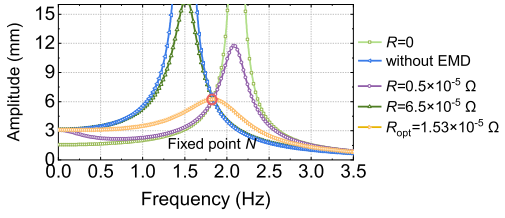

Fig. 20. Frequency response of EMD using different resistors *R*.

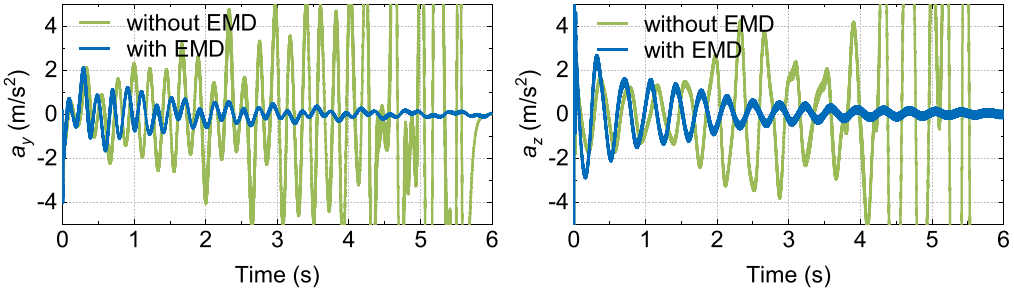

(a) Lateral acceleration (b) Vertical acceleration

Fig. 21. Comparison of the acceleration with and without the EMD.

(2) Introducing Primary Electromagnetic Dampers in the Suspension System

The induced magnetic field in the LGCs of the superconducting EDS aligns with the travel speed, providing a stable magnetic environment for non-contact electromagnetic dampers (EMD). Ohashi et al. introduced a series of passive and active damping coils (DCs) [68,69] and studied their impact on dynamic performance. The vibrations of the suspension bogie are effectively suppressed. To address the voltage lag issues, they also researched the semi-active control of DCs using an improved switching principle that accounts for motion energy. They optimized the parameters and control methods for DCs, achieving effective damping performance for both vertical-pitching [70] and lateral-rolling [71] vibrations. Additionally, they improved the weight [72], shape, and installation positions [73], switching period [74] of the DCs. Hu et al. [75] applied velocity and acceleration proportional force control on EMD to improve the dynamic performance of suspension bogie. Active or semi-active control of EMDs adjusts the damper's status using real-time sensor feedback and algorithms, which require external energy. In addition, the reliability decreases in strong magnetic fields, increasing costs and environmental impact.

Specially designed passive DCs with more stable and cost-effective working characteristics can effectively suppress vibrations and should be given special attention. Our group [76] optimized the DCs in HTS pinning maglev based on the fixed-point theory to achieve balanced performance across frequency domains. This method is suggested to optimize the DCs of the EDS suspension bogie, as shown in Fig. 20. When the resistance is zero, the curve has a peak with a large value because the vibration energy cannot be dissipated through resistance, resulting in zero damping. When the resistance is infinitely large, the damping ratio is infinitely large, and no current passes through the resistance, leading to no energy dissipation. It is important to note that all curves converge at a specific point *N*, called the fixed point, similar to mechanical dampers in behavior. Through parameter optimization, the ordinate of the fixed-point *N* can be the extreme value of the system's vibration amplitude.

Fig. 21 shows the lateral and vertical acceleration with and without the EMD under the free vibration of the suspension bogie. The initial lateral and vertical offsets are 10 mm and −40 mm, respectively. The operating velocity is 500 km/h. The vibration acceleration attenuation effect of the suspension system with EMD is significant. After 3 s, the lateral vibration acceleration decreases to 0.34 m/s^2, and the vertical vibration acceleration decreases to 0.49 m/s^2.

Suzuki and Watanabe et al. [77,78] researched the combination of a primary linear generator as the EMD system and a secondary suspension control strategy for vibration suppression. This approach effectively reduces vibrations at the natural frequencies of the primary suspension, which is typically challenging to achieve solely through secondary suspension adjustments. Additionally, this system simplifies the overall setup by incorporating vibration control into the power collection device and generates damping forces using zero-phase current flowing through the power collecting coils. The initial experiments of the linear generator attached to the bogie of full-scale EDS vehicles were conducted on the Yamanashi Maglev test line. It demonstrated the presence of electromagnetic force with an alternating current [79] and the feasibility of suppression vibration over a wider frequency range. Yan et al. [80] established a 14-degree-of-freedom maglev vehicle model, using the maximum force of EMD in the primary suspension and sky-hook damping collaborative control strategy in the secondary suspension to suppress the vibrations of the EDS train.

In summary, integrating a secondary suspension system between the car body and the bogies effectively mitigates vibrations in maglev vehicles. Nonetheless, primary EMDs are crucial for reducing high-frequency and natural-frequency vibrations in the suspension bogies, which are critical for the magneto-thermal stability of the SCMs. Notably, optimizing parameters, as illustrated in Fig. 20, can significantly enhance vibration damping across a broad frequency spectrum.

5. The application prospects of the slide window method in electromechanical coupling calculations

The electromechanical systems of EDS trains are inherently coupled, with vibrations in the vehicle affecting the induced EMF in the coils, thereby altering the electromagnetic forces. This interplay can lead to further vibrations in the vehicle, illustrating the complex feedback mechanism within the system. Suppose DCs and PCs are added to the numerical models. The computational complexity will increase significantly, making it challenging to perform dynamics simulations under high speed and various operating conditions. The sliding window method offers a promising approach to enhance computational efficiency in such scenarios and is thus worth introducing in dynamic analysis.

When a vehicle operates, various factors can lead to vibrations propagating along the track but stopping after a certain distance due to damping effects. The sliding window method for vehicle-track coupling modeling in rail transit dynamics [81] calculates the track section involved in the vibration as the vehicle moves, adjusting the track section based on vibration propagation while maintaining the overall length of the involved track. This method is also suitable for EDS train dynamics modeling, which considers only the track coils directly facing the onboard SCMs affecting the system's electromagnetic and dynamic characteristics. Ground coils far from the onboard SCMs are excluded from the electromechanical coupling effects, making them effective for simulating the interaction between the long-track coils and the onboard coils.

The main concept of the sliding window calculation method for long track coils of superconducting EDS trains is shown in Fig. 22: At time t_1, the calculation window for the LGC track is A_1B_1, which includes one suspension bogie position determination coil. The effective window section involves $(2n_0 + 1)$ groups of 8-shaped LGCs with a practical electromechanical coupling effect. While the influence of

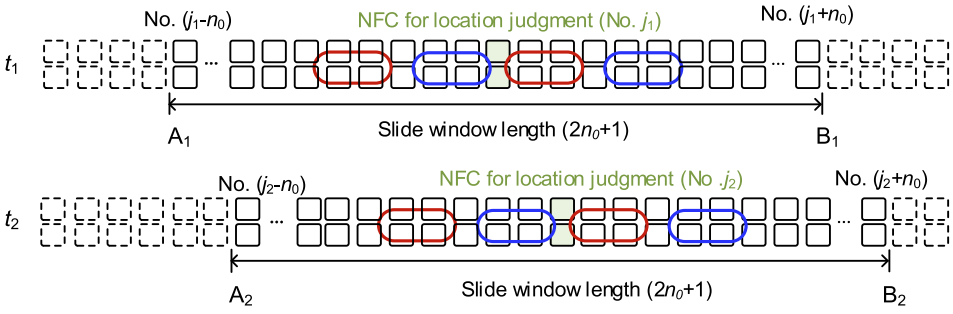

(a) The principle of applying the sliding window method to EDS suspension bogie

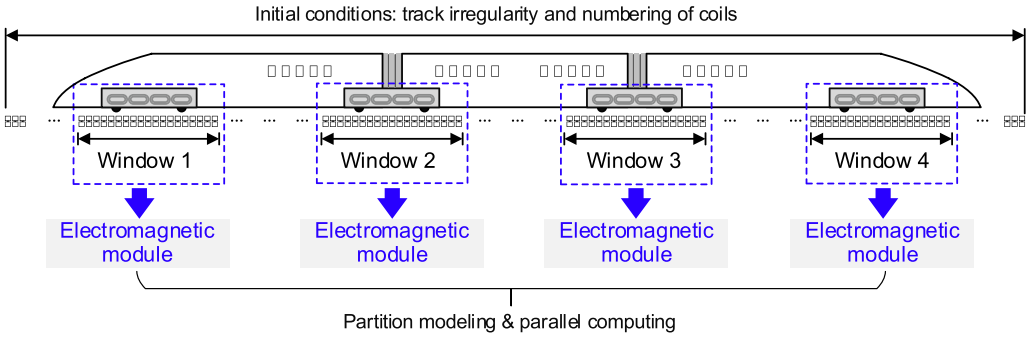

(b) Schematic diagram of sliding window method applied to 3-car and 4-bogie EDS vehicles

Fig. 22. Sliding window method applied to EDS system.

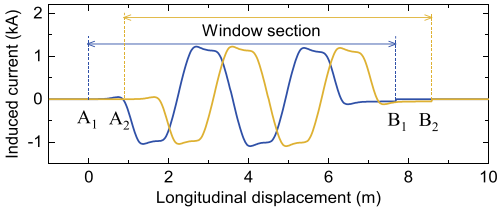

Fig. 23. Schematic diagram of induced current in LGC loop in the sliding window section.

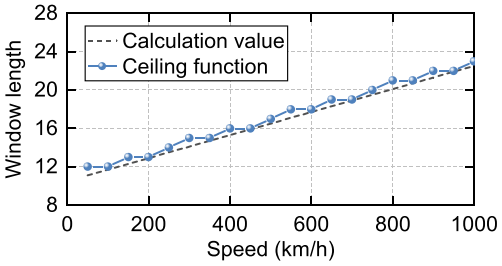

Fig. 24. Relationship between sliding window length and running speed.

other LGCs can be disregarded. At time t_2, the calculation window shifts to A_2B_2, and the number of LGC groups remains ($2n_0$ + 1). The LGCs outside the sliding window section do not participate in the calculation.

Fig. 23 illustrates the induced current in the LGCs when applying the sliding window method. The current in coils outside the window is zero, which markedly reduces the matrix size needed for inductance and circuit differential equations.

When selecting an appropriate window length, balancing accuracy and computation time is crucial. It is assumed that after the onboard SCM passes over a certain 8-shaped LGC, there is no external field change, and the current I_j decays exponentially, i.e., $I_j = I_0 e^{-t/\tau}$ with a time constant τ of 0.0389 s (L = 0.288 mH, R = 7.6 Ω). When simulating at higher operating speeds, a longer window should be selected. Based on the electromagnetic time constant, the relationship between the selectable window length (i.e., the number of the LGCs in the window section) and the operating speed is shown in Fig. 24.

6. Conclusion

In conclusion, this article presents a comprehensive overview of the research progress, electromagnetic modeling, dynamic analysis, and experimental method and platform in superconducting EDS systems. It discusses various modeling and simulation methods, validation techniques, and potential optimization strategies. The principal contributions and conclusions of this study are summarized below:

(1) Finite element models have proven highly effective for analyzing electromagnetic coupling in 8-shaped LGCs and onboard SCMs. The introduction of periodic boundary conditions for modeling long-track sections allowed for efficient simulations of electromagnetic coupling effects while maintaining computational accuracy.

(2) Using the dynamic circuit theory, commonly employed in electromagnetic analysis models, led to a general expression for mutual inductance between rectangular coils and racetrack-shaped coils based on Neumann's formula. The study recommends discretizing coil loops, 32 segments for LGCs and 64 for SCMs, to balance computational precision with efficiency.

(3) A comparison and validation of mutual inductance calculations between the FEM and the discrete Neumann's formula method were conducted, with the latter yielding slightly larger results. When compared with experimental data, the FEM's electromagnetic force calculations demonstrated superior accuracy over the dynamic circuit model.

(4) Equivalent testing platforms were discussed, including static simulations involving active current excitation of LGCs, dynamic simulations using rotational motion to replace linear motion and dynamic performance simulations based on Stewart platforms. A platform capable of facilitating cross-connection LGCs and passive suspension was elaborated, highlighting its value in dynamic characteristic analysis.

(5) Inherent damping provided by the interaction between the onboard SCMs and the LGCs is negative, necessitating additional damping design to ensure dynamic stability and passenger comfort. The induction magnetic field generated by the LGC during train operation can be utilized to construct primary EMDs. The article introduces the fixed-point theory to achieve balanced damping across a wide frequency.

(6) The sliding window method was introduced to superconducting EDS systems and was outlined, offering a significant boost in computational efficiency of vehicle dynamic analysis. The correlation between the chosen length of the sliding window and the operational speed of simulations is also presented.

However, dynamic characteristics analysis of superconducting EDS systems remains a complex yet promising area of research. Challenges in modeling, simulation, and optimization persist. The system's nonlinearity and the complex coupling of electromagnetic and mechanical systems demand advanced mathematical models and computational techniques to ensure accurate dynamic performance prediction. Future research should aim to further integrate and optimize models of superconducting EDS systems to handle a broader range of operational conditions and configurations. For higher precision simulations, aspects such as the propulsion system, control systems, and aerodynamics could be further incorporated into dynamic models.

In addition, strengthening collaboration between academia and industry is crucial for advancing this technology. Currently, the availability of experimental data is quite limited, which restricts theoretical research. The industrial sector could accelerate the practical application of discoveries by sharing research outcomes, resources, and experimental facilities. Simultaneously, the latest simulation results from academia can be promptly utilized for engineering validation and application.

CRediT authorship contribution statement

Huan Huang: Writing – original draft, Methodology, Investigation, Data curation. **Haitao Li:** Writing – review & editing, Conceptualization. **Tim Coombs:** Supervision. **Hanlin Zhu:** Software, Methodology. **Yougang Sun:** Formal analysis. **Guobin Lin:** Funding acquisition. **Junqi Xu:** Project administration. **Jun Zheng:** Writing – review & editing.

Declaration of competing interest

The authors declare that they have no known competing financial interests or personal relationships that could have appeared to influence the work reported in this paper.

Acknowledgement

This work was supported in part by the China Postdoctoral Science Foundation (2024M752424) and National Natural Science Foundation of China (52305133, 52232013).

References

[1] Han H, Kim D. Magnetic levitation. Dordrecht: Springer; 2016.
[2] Powell J, Danby G. A 300 mph magnetically suspended train. Mech Eng 1967;89:30–5.
[3] Motoharu O, Shunsaku K, Hisao O. Japan's superconducting Maglev train. IEEE Instrum Meas Mag 2002;5(3):9–15.
[4] JR-Central. About the Yamanashi Maglev Line. (2022-12-01) [2023-12-26]. https://scmaglev.jr-central-global.com/maglevline/about/.
[5] Terai M. The R&D project of HTS magnets for the superconducting Maglev. IEEE Trans Appl Supercond 2007;16(2):1124–9.
[6] Kusada S. The project overview of the HTS magnet for superconducting Maglev. IEEE Trans Appl Supercond 2007;2(17):2111–6.
[7] Mizuno K, Ogata M, Hasegawa H. Manufacturing of a REBCO racetrack coil using thermoplastic resin aiming at Maglev application. Physic C 2015;2015 (518):101–5.
[8] Yao C, Ma Y. Superconducting materials: challenges and opportunities for large-scale applications. iScience 2021;24(6):102541.
[9] Miyazaki Y, Ikeda K, Mizuno K, et al. Development of an on-board cooling system with multiple pulse-tubes for HTS Maglev. Teion Kogaku 2013;48(7):377–81 (in Japanese).
[10] Choi SY, Lee CY, Jo JM, et al. Sub-sonic linear synchronous motors using superconducting magnets for the Hyperloop. Energies 2019;12(24):4611.
[11] Lim J, Lee C, Oh YJ, et al. Equivalent inductance model for the design analysis of electrodynamic suspension coils for the Hyperloop. Sci Rep 2021;11:23499.
[12] Lee C, Lee J, Lim J, et al. Design and evaluation of prototype high-Tc superconducting linear synchronous motor for high-speed transportation. IEEE Trans Appl Supercond 2020;30(4):3602205.
[13] China set to test 1,000 km/h ultra-high-speed maglev train. (2023-04-24) [2024-04-25]. https://news.cgtn.com/news/2023-04-24/China-set-to-test-1-000km-h-ultra-high-speed-maglev-train-1jgCFqBvmq4/index.html.
[14] The commercial aerospace electromagnetic launch high-temperature superconducting electrodynamic suspension navigation test was a complete success!. (2023-09-11) [2024-04-26]. http://maglev-pt.org.cn/index.php?m=home&c=View&a=index&aid=313.
[15] Yu Q, Li K, Hu H, et al. Research and technological prospects of applications for superconducting electrodynamic suspension. Electric Drive for Locomotives 2023;4:1–8 (in Chinese).
[16] S. Liu, L. Wang, Y. Chen, et al. R&D of on-board metal-insulation REBCO superconducting magnet for electrodynamic suspension system. 2023, 36: 064002.
[17] Murai T, Fujimoto T, Fujiwara S. Test run of combined propulsion, levitation and guidance system at Miyazaki test track. Electr Eng Jpn 1996;117(2):68–79.
[18] Fujimoto T, Aiba M, Suzuki H, et al. Characteristics of electromagnetic force of ground coil for levitation and guidance at the Yamanashi Maglev test line. Quart Rep Railway Techn Res Inst 2000;41(2):63–7.
[19] He JL, Rote DM. Double-row loop-coil configuration for EDS Maglev. IEEE Trans Magn 1993;29(6):2956–8.
[20] Cai Y, Ma G, Wang Y, et al. Semianalytical calculation of superconducting electrodynamic suspension train using figure-eight-shaped ground coil. IEEE Trans Appl Supercond 2020;30(5):3602509.
[21] He J, Rote D, Coffey H. Applications of the dynamic circuit theory to Maglev suspension systems. IEEE Trans Magn 1993;29(6):4153–63.
[22] Fujiwara S, Fujimoto T. Characteristics of combined levitation and guidance EDS Maglev system. Electr Eng Jpn 1993;113(3):123–34.
[23] Gong T, Ma G, Wang R, et al. 3-D FEM modeling of the superconducting EDS train with cross-connected figure-eight-shaped suspension coils. IEEE Trans Appl Supercond 2021;31(3):3600213.
[24] Chen D, Li X, Huang X, et al. An FEM model for evaluation of force performance of high-temperature superconducting null-flux electrodynamic Maglev system. IEEE Trans Appl Supercond 2021;31(7):3603806.
[25] Huang H, Zhu H, Coombs T, et al. FE modeling of superconducting EDS system employing mixed formulations and field-circuit coupling method. IEEE Trans Transp Electrif 2023;9(1):1618–28.
[26] Azukizawa T. Persistent current analysis of superconducting coils in an electrodynamic suspension system. Electr Eng Jpn 1995;115(2):432–7.
[27] S. Wan, J. Qian, G. Ni, et al. Study of the levitation and guidance technology for electrodynamic suspension maglev vehicle. 2000(9): 22-31 (in Chinese).
[28] Y. Li, W. Yang, M. Ye, et al. Calculation and analysis of maglev levitation and guidance system in magnetic launch-assist system. 2018, 39(5): 54-60 (in Chinese).
[29] Zhang J, Zhao C, Feng Y, et al. Study on mechanical characteristics of the electrodynamic levitation and guidance system for the superconducting Maglev train. Machinery 2020;47(9):25–32.
[30] Mirzaei M. Calculations of self- and mutual inductances for racetrack coils using equivalent models. IEEE Trans Transp Electrif 2023;9(2):2177–84.
[31] Nonaka S, Hirosaki T, Kawakami E. Analysis of characteristics of repulsive magnetic levitated train using a space harmonic technique. Electr Eng Jpn 1980;100(10):601–8.
[32] Lv G, Liu Y, Zhang Z, et al. Characteristic analysis of coreless-type linear synchronous motor with the racetrack coils as secondary for EDS Maglev train. IEEE/ASME Trans Mechatron 2022;27(6):4654–64.
[33] Lv G, Zhang Z, Liu Y, et al. Analysis of forces in linear synchronous motor with propulsion, levitation and guidance for high-speed Maglev. IEEE J Emerg Sel Top Power Electron 2022;10(3):2903–11.
[34] Zhu H, Zheng J, Fu S, et al. Numerical mutual inductance model based on spatial Fourier decomposition for racetrack coils in EDS system. IEEE Trans Energy Convers 2024;online(0):1–14.
[35] Mizuno K, Sugino M, Tanaka M, et al. Experimental production of a real-scale REBCO magnet aimed at its application to Maglev. IEEE Trans Appl Supercond 2017;27(4):3600205.
[36] G. Lu, X. L. Guo. Calculation of power generation characteristics of linear harmonic generator for electrodynamic suspension maglev train. 2023, 4(58): 783-791 (in Chinese).

[37] The Development of Linear Generator System Combined with Magnetic Damping Function. 2006.
[38] Kim K, Levi E, Zabar Z, et al. Mutual inductance of noncoaxial circular coils with constant current density. IEEE Trans Magn 1997;33(5):4303–9.
[39] Su Z, Luo J, Ma G, et al. Fast and precise calculation of mutual inductance for electrodynamic suspension: methodology and validation. IEEE Trans Ind Electron 2022;69(6):6046–57.
[40] Brambilla R, Grilli F, Martini L, et al. A finite-element method framework for modeling rotating machines with superconducting windings. IEEE Trans Appl Supercond 2018;28(5):5207511.
[41] Santos BMO, Dias FJM, Sass F, et al. Simulation of superconducting machine with stacks of coated conductors using hybrid A-H formulation. IEEE Trans Appl Supercond 2020;30(6):5207309.
[42] Jin J. The finite element method in electromagnetics. New York: John Wiley & Sons; 1993.
[43] Tanaka M, Aiba M, Suzuki M. Development of electromagnetic vibration test apparatus for ground coils applied to Maglev system. Quart Rep Railway Techn Res Inst 2017;48(2):110–4.
[44] Matsue H, Aiba M, Suzuki M. Stress evaluation of the PLG ground coil with GFRP fastening devices. Japan: Niigata; 2009.
[45] Mizuno K, Tanaka M, Ogata M. Evaluation of eddy current heating in a REBCO magnet due to the magnetic field of ground coils for the maglev. Supercond Sci Technol 2020;33(7):074009.
[46] Ma G, Wang Y, Luo J, et al. An analytical-experiment coupling method to characterize the electrodynamic suspension system at various speeds. IEEE Trans Ind Electron 2022;69(7):7170–80.
[47] D. Y. Hu, S. Q. Yan, H. Cai, et al. The design of an electromagnetic vibration test bench for maglev superconducting magnets. 2023, 23(6): 193-205 (in Chinese).
[48] Suzuki E, Watanabe K, Hoshino H, et al. A study of Maglev vehicle dynamics using a reduced-scale vehicle model experiment apparatus. J Mech Syst Transport Logist 2010;3(1):196–205.
[49] Lee J, You W, Lim J, et al. Development of the reduced-scale vehicle model for the dynamic characteristic analysis of the Hyperloop. Energies 2021;14(13):3883.
[50] Song M, Zhou D, Yu P, et al. Analytical calculation and experimental verification of superconducting electrodynamic suspension system using null-flux ground coils. IEEE Trans Intell Transp Syst 2022;23(9):14978–89.
[51] Wang Y, Cai Y, Song X, et al. Characteristic analysis and experiment of the equivalent simulation system for null-flux electrodynamic suspension. Trans China Electrotechn Soc 2021;36(8):1628–35.
[52] Rote DM, Cai Y. Review of dynamic stability of repulsive-force Maglev suspension systems. IEEE Trans Magn 2002;38(2):1383–90.
[53] Higashi K, Ohashi S, Ohsaki H, et al. Magnetic damping of the electrodynamic suspension-type superconducting levitation system. Electr Eng Jpn 1999;127 (2):1015–23.
[54] Hu D, Feng X, Zhang Z. Study on the damping characteristics of superconducting electrodynamic suspension system. Proc CSEE 2021;41(13):4679–88 (in Chinese).
[55] Yonezu T, Watanabe K, Suzuki E. Characteristics of magnetic springs for guidance of superconducting Maglev vehicles. Quart Rep Railway Techn Res Inst 2018;59 (4):293–8.
[56] Yoon R, Negash BA, You W, et al. Capsule vehicle dynamics based on levitation coil design using equivalent model of a sidewall electrodynamic suspension system. Energies 2021;14(16):4979.
[57] Yu Q, Wang M, Yao G, et al. Study on beat vibration of a high temperature superconducting EDS Maglev vehicle at low speed. Appl Sci 2023;13(5):3131.
[58] Xiaoxu Z, Sai Z, Weihua MA, et al. Dynamic model of superconducting electric levitation vehicle. Machinery 2022;49(10). 35–41, 57.
[59] Ha H, Park J, Park K. Advanced numerical analysis for vibration characteristics and ride comfort of ultra-high-speed maglev train. Microsyst Technol 2020;26 (1):183–93.
[60] Li H, Zhu H, Huang H, et al. A new suppression strategy of pitching vibration based on the magnetic-electric-mechanical coupling dynamic model for superconducting EDS transport system. Mech Syst Sig Process 2023;188:110039.
[61] Ohashi S, Ohsaki H, Masada E. Running characteristics of the superconducting magnetically levitated train in the case of superconducting coil quenching. Electr Eng Jpn 2000;130(1):937–46.
[62] Tan Y, Zhou D, Li J, et al. Dynamic simulation analysis of null-flux coil superconducting electrodynamic suspension system. IEEE Trans Intell Veh 2023;9(1):1005–16.
[63] Ma G, Yan Z. Vehicle-track coupled dynamics model for superconducting electrodynamic suspension train. Veh Syst Dyn 2023;61(12):3202–24.
[64] Su Z, Luo J, Feng P, et al. Vertical-lateral coupled dynamic model for integrated propulsion, levitation and guidance superconducting EDS train. IEEE Trans Intell Transp Syst 2023. https://doi.org/10.1109/TITS.2023.3330421.
[65] Sakamoto T, Nakayama M. Levitation-guidance stabilization of superconducting maglev through LSM currents. Math Comput Simul 2006;71(4):404–14.
[66] Boeij JD, Steinbuch M, Gutierrez H. Mathematical model of the 5-DOF sled dynamics of an electrodynamic Maglev system with a passive sled. IEEE Trans Magn 2005;41(1):460–5.
[67] Gutierrez HM, Luijten H. 5-DOF real-time control of active electrodynamic Maglev. IEEE Trans Ind Electron 2018;65(9):7468–76.
[68] Ohashi S. Effect of the damper coils on the rotational motion of the superconducting magnetically levitated bogie. IEEE Trans Magn 2000;36 (5):3680–2.
[69] Ohashi S. Effect of the active damper coils of the superconducting magnetically levitated bogie in case of acceleration. IEEE Trans Magn 2008;44(11):4163–6.
[70] Ohashi S, Ueshima T. Control method of the semi-active damper coil system in the superconducting magnetically levitated bogie against vertical and pitching oscillation. IEEE Trans Magn 2012;48(11):4542–5.
[71] Ohashi S, Nakakida R, Takeuchi T. Control of the lateral vibration by using weight reduced damper coil on superconducting magnetically levitation bogie. Neuchatel, Switzerland: IEEE; 2019.
[72] Ohashi S. Weight reduction of the damper coils in the superconducting magnetically levitated bogie. IEEE Trans Magn 2018;54(11):8300104.
[73] Yamamoto R, Betsunoh R, Ohashi S. Improvement of damping factor by optimal shape and installation position of the damper coils at low velocity range in electrodynamic suspension system. J Phys Conf Ser 2022;2323(1):012038.
[74] Betsunoh R, Ohashi S. Stable levitation in the low velocity range with the damper coils in electrodynamic suspension system. IEEE Trans Ind Appl 2021;57 (6):7046–53.
[75] D. Hu, X. Feng, X. Ma, et al. Study on vertical vibration suppression methods of superconducting electrodynamic suspension system with a field-circuit-motion model. *Proceedings of the CSEE*. 2023, 43(10): 3972-3986 (in Chinese).
[76] Li H, Deng Z, Huang H, et al. Theoretical optimization and experimental verification of a non-contact damper for high temperature superconducting Maglev systems. J Vib Control 2022;28(5–6):606–14.
[77] Watanabe K, Yoshioka H, Suzuki E. Combined control of primary and secondary suspension of Maglev vehicles. Quart Rep Railway Techn Res Inst 2004;45 (1):26–31.
[78] Watanabe K, Yoshioka H, Suzuki E, et al. A study of vibration control systems for superconducting Maglev vehicles (vibration control of lateral and rolling motions). J Syst Des Dyn 2007;1(3):593–604.
[79] Suzuki E, Watanabe K. Results of vibration control of a Maglev vehicle utilizing a linear generator. California, USA: ASME; 2005.
[80] Yan Z, Li G, Luo J, et al. Vibration control of superconducting electro-dynamic suspension train with electromagnetic and sky-hook damping methods. Veh Syst Dyn 2022;60(10):3375–97.
[81] W. Zhang. Research on service simulation modeling and calculation method of high-speed train. 2021, 53(1): 96-104 (in Chinese).